

Supplementary Information

On the importance of pyrolysis for inkjet-printed oxide piezoelectric thin films

Nicolas Godard,^{*a} Mohamed Aymen Mahjoub,^a Stéphanie Girod,^a
Tony Schenk,^a Sebastjan Glinšek,^a and Emmanuel Defay^a



Fig. S1 – Wetting of PZT ink on platinized silicon. A $\sim 1 \mu\text{L}$ droplet was deposited on a platinized silicon substrate degassed at $350 \text{ }^\circ\text{C}$ for 5 min. Complete wetting occurs within seconds.

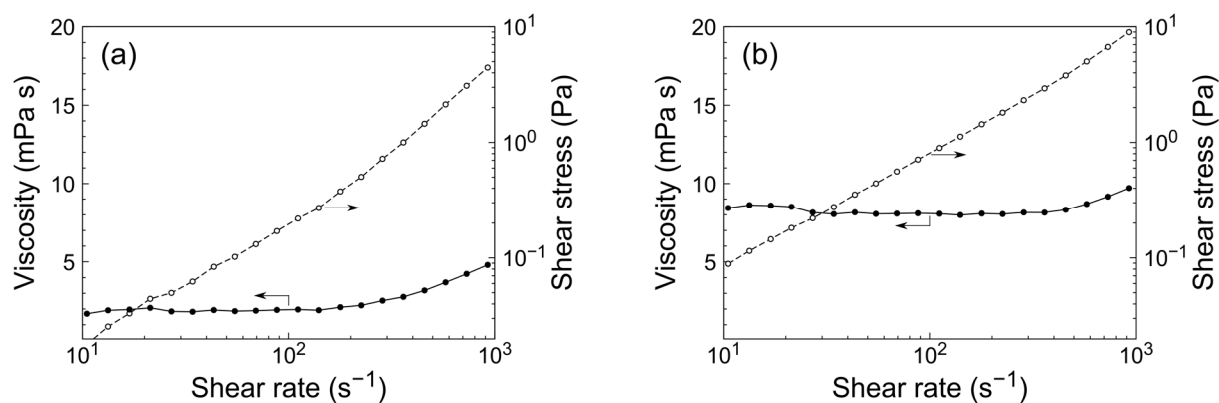


Fig. S2 – Flow curves of (a) the PZT spin coating solution and (b) PZT ink. The values reported in Table 1 are the ones obtained for a shear rate of 100 s^{-1} .

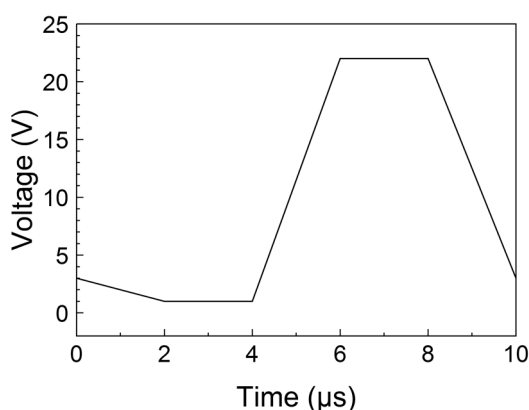


Fig. S3 – Pulse waveform used for jetting PZT ink with Dimatix® DMCLCP-11610 cartridges (10 pL nominal volume).

^a Materials Research and Technology department, Luxembourg Institute of Science and Technology, rue du Brill 41, L-4422 Belvaux, Luxembourg; Tel: +352 275 885; Email: nicolas.godard@list.lu

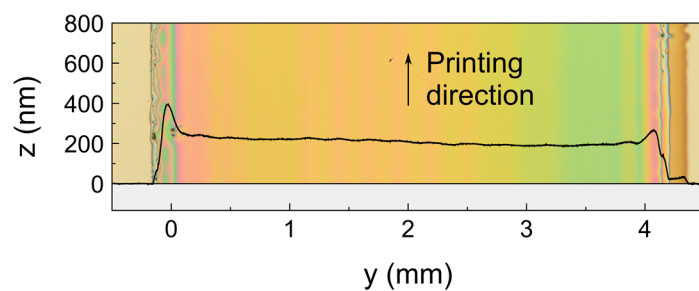


Fig. S4 – Optical micrograph combined with profilometry measurement of a 4 mm-wide inkjet-printed PZT stripe.

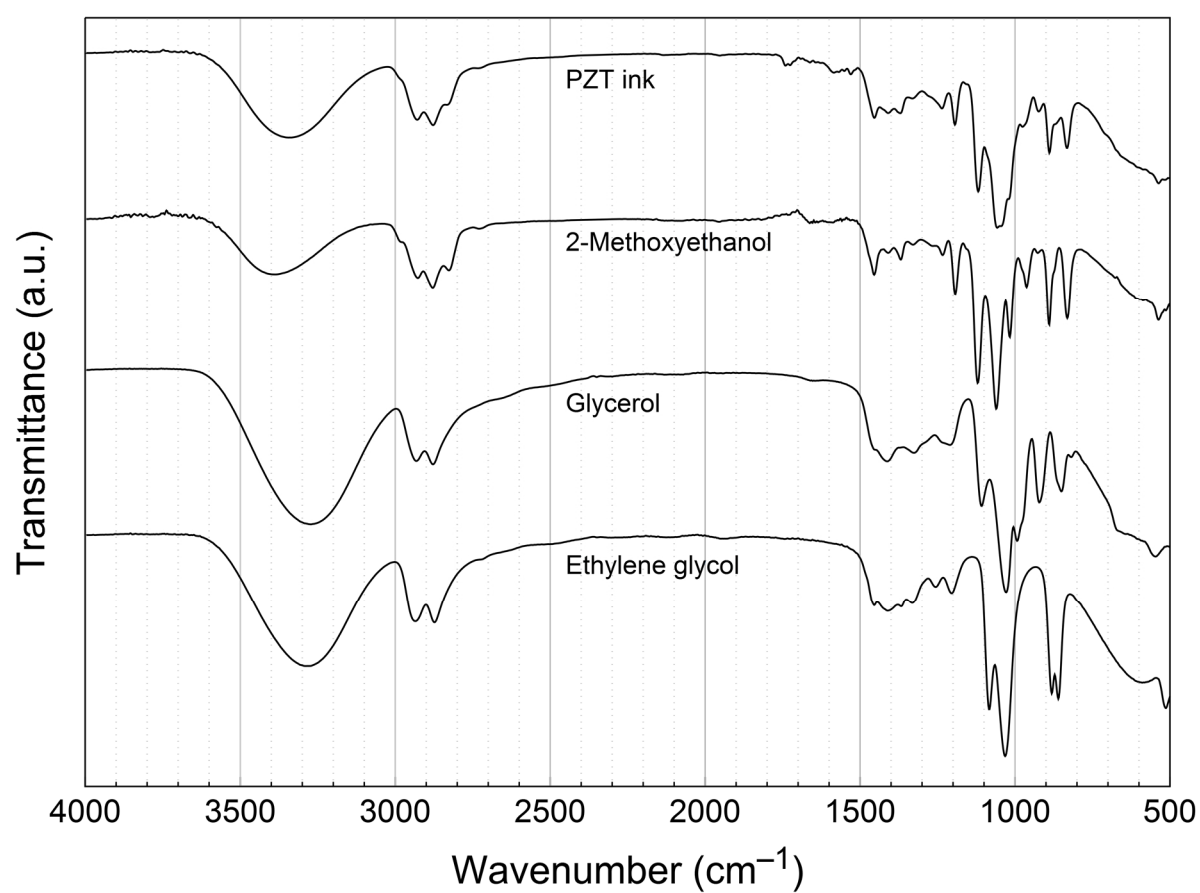


Fig. S5 – FTIR spectra of the PZT ink and pure constitutive solvents (acquired in ATR mode).

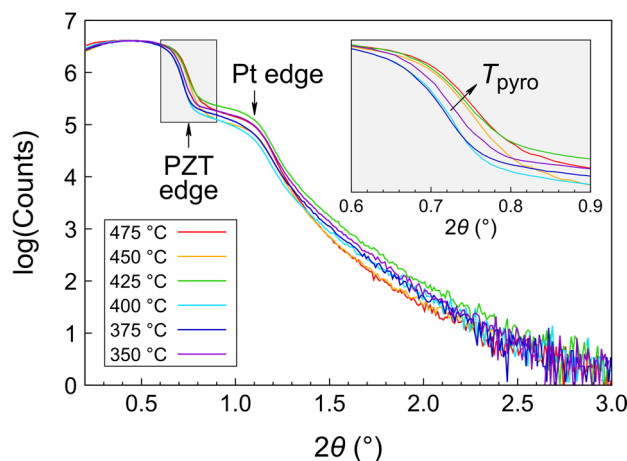


Fig. S6 – X-ray reflectivity patterns of crystallized inkjet-printed PZT films pyrolyzed for 3 min at temperatures ranging from 350 °C to 475 °C. A close-up of the shaded area is shown in the inset.

Note on X-ray reflectivity measurements

X-ray reflectivity (XRR) was used to assess the porosity trend derived from SEM cross section images (Fig. 4a). The critical angle of total reflection θ_c is directly linked to the mass density ρ of the PZT films and gives rise to an abrupt intensity drop in a plot of log intensity versus 2θ .^{s1}

XRR patterns were recorded using a PANalytical X'Pert Pro diffractometer with Cu-K α radiation (0.154 nm wavelength). Our instrumental setup does not offer a micro-spot with corresponding sophisticated alignment options. To achieve the smallest possible footprint of the X-ray beam with the present instrument, the width of the beam was confined to about 4 mm using a mask (steel slide with a vertical slit as provided by PANalytical) and a knife-edge collimator was employed to limit the length of the beam footprint.

Nonetheless, the evaluation of the measured curves is significantly impacted by the irregular sample geometry (stripes with edge effects, as shown in Fig. S4, instead of a closed film of homogeneous thickness). Therefore, a fit of the full XRR curve was not possible and only the edge region related to PZT density was assessed. Absolute density values are not trustworthy as will be explained below. However, relative changes are reliable as the sample geometry affects all recorded patterns in a similar way.

The critical angle θ_c was defined via an intensity drop to 50 % of the intensities found at $2\theta = 0.4$ to 0.5° , a plateau-like region of total the reflection regime that is outside the lower-angle region affected by footprint effects but still sufficiently far away from the edge. The density was calculated from θ_c as explained by Gibaud and Vignaud¹ using atomic scattering factors available in the following references: ^{s2-s4}. Note that the second edge found at 2θ around 1.1° is related to the platinum under printed PZT stripes, which has a much larger density.

The variation in θ_c obtained from using 0.4 , 0.45 or 0.5° as initial intensity was used to derive an uncertainty estimate of $\pm 0.1 \text{ g cm}^{-3}$ in density. Another $\pm 0.1 \text{ g cm}^{-3}$ was added to this estimate based on the uncertainty of $\pm 0.005^\circ$ stemming from the finite step width of the XRR scan.

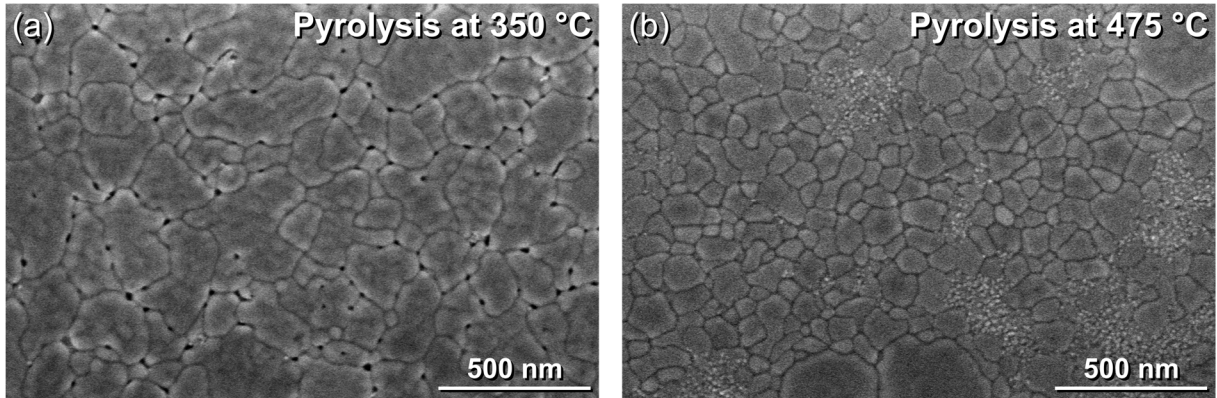


Fig. S7 – SEM micrographs of the surface of inkjet-printed PZT films pyrolyzed at (a) 350 °C and (b) 475 °C, then crystallized at 700 °C. The film pyrolyzed at 350 °C clearly exhibits intergranular porosity.

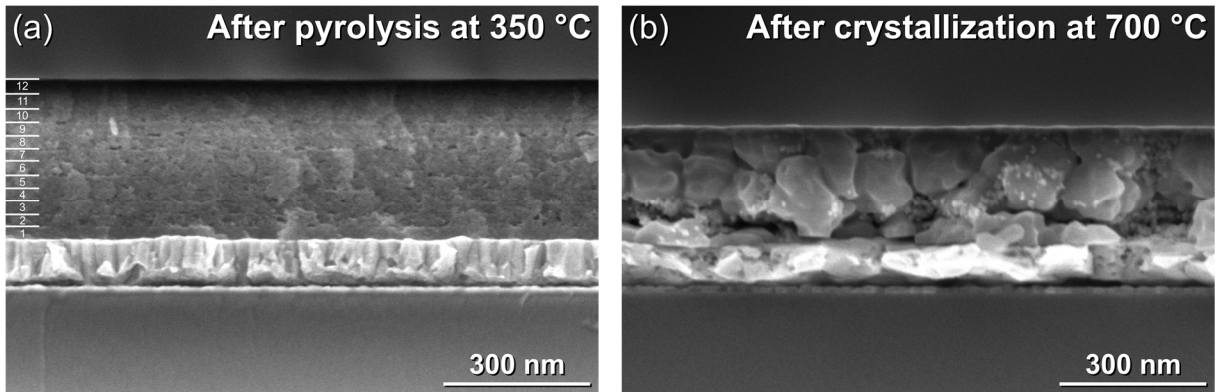


Fig. S8 – SEM micrographs of the cross section of inkjet-printed PZT films pyrolyzed at (a) 350 °C and then (b) crystallized at 700 °C. Significant porosity develops during the high-temperature annealing step, as the result of evolution of gaseous by-products. The layer succession is visible in the pyrolyzed film and disappears during crystallization, accompanied by shrinkage of the film in the order of 25%.

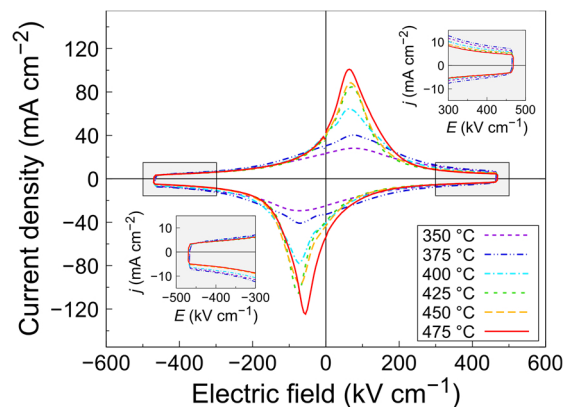


Fig. S9 – Current loops corresponding to the P - E loops illustrated in Fig. 5a (measured at 100 Hz). Insets in the bottom left and top right quadrants present a magnified view of the highlighted areas.

Table S10 – Comparison of the electrical properties of inkjet-printed PZT presented in this study with the literature.

Reference	Year	Process	Thickness (μm)	P_r ($\mu\text{C cm}^{-2}$)	E_c (kV cm^{-1})	ε'	$\tan \delta$
Fang et al. ^{s5}	2006	Spin coating	1.64	14	30	–	–
Bathurst et al. ^{s6}	2009	Inkjet printing	0.4	8.5	110	–	–
Moriomoto et al. ^{s7}	2010	Sputtering	2.8	30	50	166	–
Pérez et al. ^{s8}	2010	Spin coating	0.42	15	50	1000	0.05
Rho et al. ^{s9}	2010	Spin coating	0.36	20	30	1100	–
Machida et al. ^{s10}	2012	Inkjet printing	2	10	17	1700	0.05
Zuo et al. ^{s11}	2012	Pulsed laser deposition	0.2	25	55	2650	–
Borman et al. ^{s12}	2017	Spin coating	1.5	32	38	1650	0.03
Godard et al. ^{s13}	2019	Inkjet printing	0.44	13	58	900	0.07
This work	2019	Inkjet printing	0.2	23	60	1000	0.04

Supplementary Note S11: Vibration of a cantilever beam structure (Euler-Bernoulli theory^{s14})

The first resonant frequency f of a cantilever beam is given by:

$$f = \frac{(1.875)^2}{2\pi} \sqrt{\frac{EI}{\lambda L^4}} \quad (1)$$

where E is the Young modulus [Pa], I is the moment of inertia about the neutral axis [m^4], λ is the mass per unit length [kg m^{-1}] and L is the length [m] of the cantilever beam.

For a cantilever beam with a rectangular cross section, the moment of inertia I can be expressed as $\frac{bh^3}{12}$. Equation (1) can be rewritten as:

$$f = \frac{(1.875)^2}{2\pi} \sqrt{\frac{Eh^2}{12\rho L^4}} \quad (2)$$

where b is the cantilever width [m], h is the cantilever thickness [m] and ρ is the density [kg m^{-3}].

Equation (2) has to be modified when a proof mass M is attached at the end of the cantilever. Let m' be the effective mass at the free end of a massless cantilever producing the same resonant frequency as the cantilever without a proof mass. Its resonant frequency f' is given by:

$$f' = \frac{1}{2\pi} \sqrt{\frac{k}{m'}} \quad (3)$$

where k is the stiffness constant [N m^{-1}] of the cantilever beam. In the considered case, $k = \frac{3EI}{L^3}$. Equation (3) becomes:

$$f' = \frac{1}{2\pi} \sqrt{\frac{3EI}{m'L^3}} \quad (4)$$

The formalism of equation (1) lets us write:

$$f' = \frac{(1.875)^2}{2\pi} \sqrt{\frac{EI}{mL^3}} \quad (5)$$

where m is the mass of the cantilever beam [kg]. Setting equation (4) equal to (5) and expressing m' as function of m yields:

$$m' = \frac{3}{(1.875)^4} m \quad (6)$$

Finally, it can be shown that the resonant frequency f_M of the cantilever with a proof mass M can be expressed in the form:

$$f_M = \frac{1}{2\pi} \sqrt{\frac{k}{M+m'}} \quad (7)$$

which gives the following expression after simplification.

$$f_M = \frac{1}{2\pi} \sqrt{\frac{Ebh^3}{4L^3 \left(M + \frac{3\rho bhL}{(1.875)^4} \right)}} \quad (8)$$

One can verify that setting $M = 0$ simply returns equation (2).

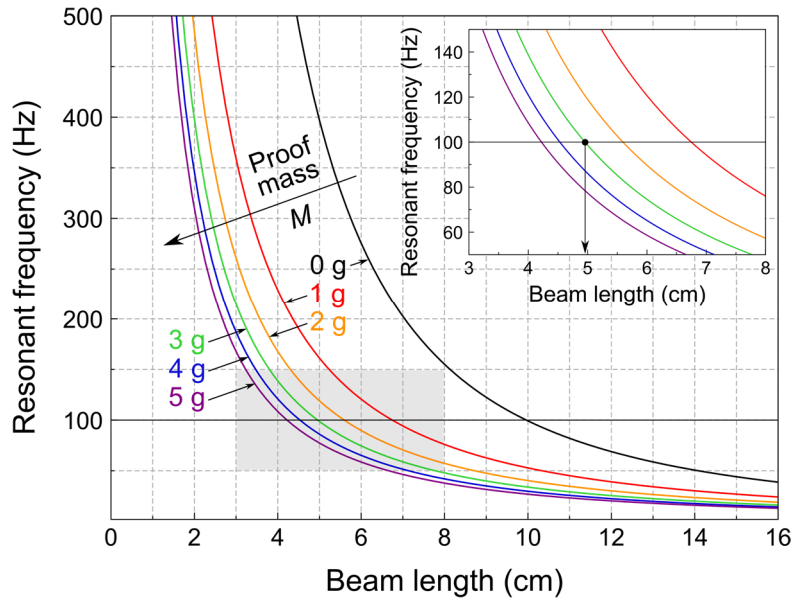


Fig. S11 – Resonant frequency as function of beam length and proof mass for a 700 μm -thick and 1 cm-wide silicon cantilever, computed using Equation (8). The inset shows a close-up view of the shaded area of the plot. According to this model, a 5 cm-long silicon cantilever with a 3 g proof mass at the tip has a resonant frequency of ~ 100 Hz.

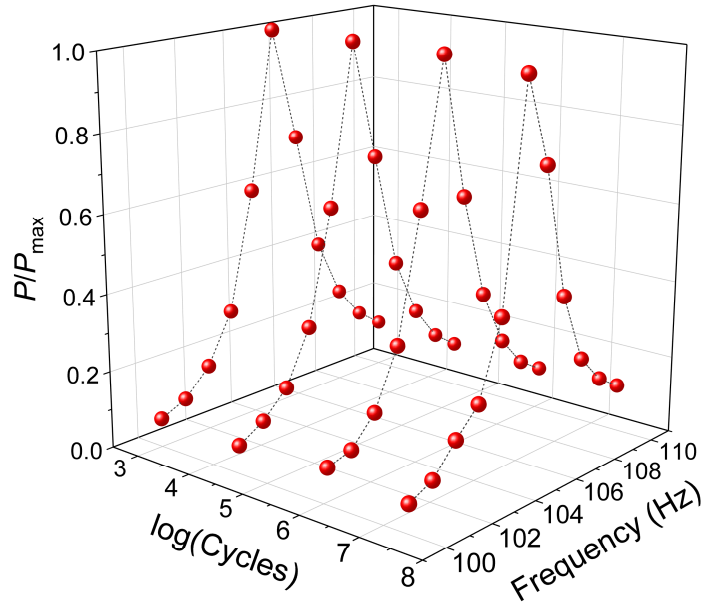


Fig. S12 – Aging test of the energy harvesting device. The normalized output power (P/P_{\max}) at resonance (here: 105 Hz) remained constant for at least $25 \cdot 10^6$ cycles. Note that the resonant frequency can be influenced by sample clamping, which explains the slightly different value reported in the manuscript (102 Hz).

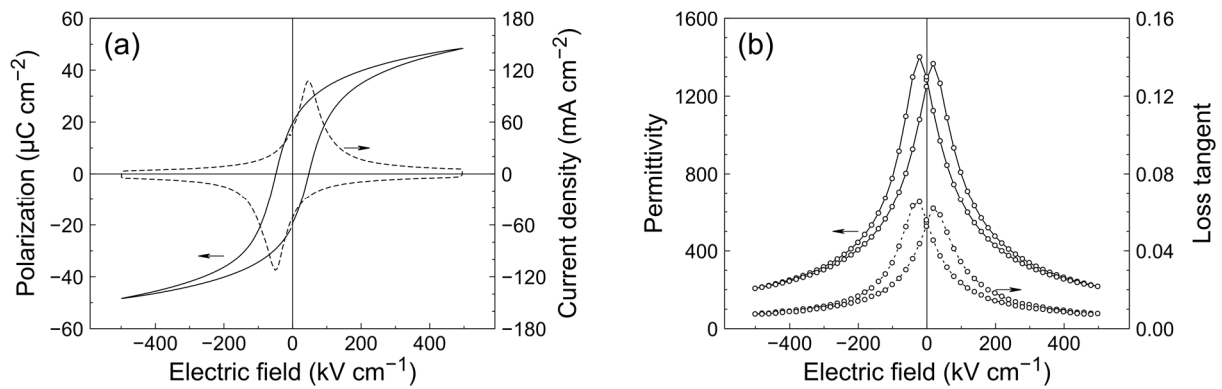


Fig. S13 – Polarization-electric field at 100 Hz and (b) permittivity-electric field loops at 1 kHz ($V_{AC} = 1$ V) measured for inkjet-printed 1 μm -thick PZT films (100 μm -diameter platinum top electrodes).

References

- s1. A. Gibaud and G. Vignaud, "Specular Reflectivity from Smooth and Rough Surfaces", *X-ray and neutron reflectivity: principles and applications* (2nd ed.), Springer, 2009, Berlin.
- s2. "The Atomic Scattering Factor Files" available from Lawrence Berkeley National Laboratory at http://henke.lbl.gov/optical_constants/ (accessed 4 December 2019).
- s3. B. L. Henke, E. M. Gullikson, J. C. Davis, "X-ray interactions: photoabsorption, scattering, transmission, and reflection at E = 50–30000 eV, Z = 1–92", *Atomic Data and Nuclear Data Tables*, 1993, **54**, 181–342.
- s4. J. F. Seely, Y. A. Uspenskii, B. Kijornrattanawanich and D. L. Windt, "Coated Photodiode Technique for the Determination of the Optical Constants of Reactive Elements: La and Tb", *SPIE Proceedings*, 2006, 63170T.
- s5. H.-B. Fang, J.-Q. Liu, Z.-Y. Xu, L. Dong, L. Wang, D. Chen, B.-C. Cai and Y. Liu, *Microelectronics J.*, 2006, **37**, 1280–1284.
- s6. S. P. Bathurst and S. G. Kim, *CIRP Ann. - Manuf. Technol.*, 2013, **62**, 227–230.
- s7. K. Morimoto, I. Kanno, K. Wasa and H. Kotera, *Sensors Actuators, A Phys.*, 2010, **163**, 428–432.
- s8. J. Pérez de la Cruz, E. Joanni, P. M. Vilarinho and A. L. Kholkin, *J. Appl. Phys.*, 2010, **108**, 114106.
- s9. J. Rho, S. J. Kim, W. Heo, N.-E. Lee, H. Lee and J. Ahn, *IEEE Electron Device Lett.*, 2010, **31**, 1017–1019.
- s10. O. Machida, A. Shimofuku, R. Tashiro, A. Takeuchi, Y. Akiyama and E. Ohta, *Jpn. J. Appl. Phys.*, 2012, **51**, 09LA11.
- s11. Z. Zuo, B. Chen, Q. F. Zhan, Y. Liu, H. Yang, Z. Li, G. Xu and R. W. Li, *J. Phys. D: Appl. Phys.*, 2015, **45**, 185302.
- s12. T. M. Borman, W. Zhu, K. Wang, S. Won, K. Peter and S. E. Trolrier-McKinstry, *J. Am. Ceram. Soc.*, 2017, **100**, 3558–3567.
- s13. N. Godard, S. Glinšek, A. Matavž, V. Bobnar and E. Defay, *Adv. Mater. Technol.*, 2019, **4**, 1800168.
- s14. W. Weaver Jr., S. P. Timoshenko, D. H. Young, *Vibration Problems in Engineering*, John Wiley & Sons, 1990, Hoboken (NJ).